The International Journal of Advanced Manufacturing Technology (2019) 102:4087–4094
https://doi.org/10.1007/s00170-019-03498-4

ORIGINAL ARTICLE

A research based on advance dual-coil electromagnetic forming method on flanging of small-size tubes

Qi Xiong[1] · Hao Huang[1] · Liangyu Xia[1] · Hongtao Tang[1] · Li Qiu[1]

Received: 1 June 2018 / Accepted: 19 February 2019 / Published online: 6 March 2019

Abstract
Using electromagnetic forming process to flanging small-size tubes has been a challenge of modern forming technology. With existing electromagnetic forming system in practical aspects, it is relatively difficult and complex process for designing and winding smaller but stronger driving coil, because of the high structural strength requirement for sustaining strong Lorentz force and the low geometrical permissibility bottlenecked by the size of tubes. To approach the mentioned complication, a practical dual-coil electromagnetic forming method had been presented thoroughly in the following article. For illustrating the basic structure of the method, the two independent driving coils were located at the end of the tube instead of inside the tube. Afterward, the two coils were respectively discharged by two power supplies. They generated entirely different Lorentz force distribution with precise and analogous time controlling. To determine the effectiveness of this method, a theoretical analysis of the forming force of the electromagnetic flanging had been approached thoroughly. Then, a full coupling model of electromagnet-structure was developed to simulate the deformation of the tube. The results showed that an obvious flanging with the maximum radial displacement of 5.08 mm could be achieved on an AA1060 aluminum tube with a thickness of 1 mm and a radius of 10 mm, on the condition of 5.8 kV and 6 kV. At the closure, the influence of the pulse width of discharge currents was discussed. All these theoretical analysis and simulation results are of great potential for designing electromagnetic forming systems and widening their applications in tube flanging.

Keywords Electromagnetic forming · Flanging · Dual-coil · Pulse width

1 Introduction

Electromagnetic forming (EMF) is a high-speed and noncontact forming technology using pulsed Lorentz force to control the deformation of the workpiece. Electromagnetic flanging is one of the most effective approaches to flange the aluminum alloys. It has a series of advantages such as higher forming speed, higher forming limit, and less spring back, when compared to the traditional stamping flanging forming [1].

Currently, most researches which focused on electromagnetic forming use repulsive forces between the driving coil and the workpiece [2–5], and the principle could be shown in Fig. 1a. In the repulsive electromagnetic forming, a pulse current was generated in the driving coil while the switch was closed. At the same time, a pulse magnetic field was generated and an eddy current was induced in the tube by the driving coil. Then, a huge repulsive force could be obtained by the cooperation of the magnetic field and the eddy current, which could form the tube. Li et al. [6] adopted repulsive forces to study the deformation of electromagnetic tube bulging. And Li et al. [7] proposed a new gradient electromagnetic forming approach based on the repulsive forces to meet the force-field requirements concerning the forming process of the variable-diameter tubes. This method can achieve the tube forming effectively, but the means of loading electromagnetic forces is relatively simple and cannot meet all the processing needs. When it comes to small-size tube, the size and the shape of the coil are limited by the structure of the tube and become a severe challenge. In the process, a smaller coil should be winded to put inside the smaller tube. And that would cause an excessive curvature of the coil that also led to a stronger stress in the wire, which would not only shorten the work life of the coil but also pose structural risks to the whole system. Therefore, this method was mainly applied to large-size tubes.

✉ Li Qiu
465863669@qq.com

[1] College of Electrical Engineering & New Energy, China Three Gorges University, Yichang 443002, Hubei, China

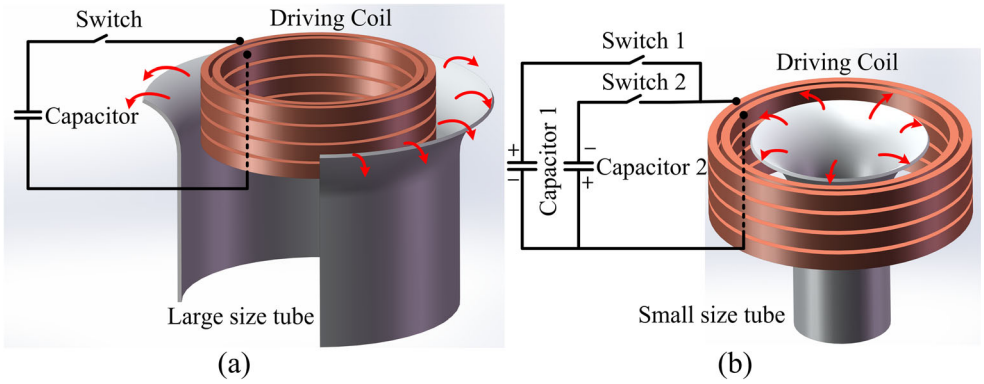

Fig. 1 Schematic diagram of electromagnetic flanging **a** repulsive force; **b** attractive force

Recently, this challenge could be tackled by an attractive electromagnetic forming system, in which the coil was placed outside the tube, as shown in Fig. 1b. The system consisted of two power supplies, in which a long pulse current and a short pulse current were loaded to one coil with precise time control. Two currents could be seen as a combination current with a slow-rise and a rapid-decline stage, and it would generate an attractive force strong enough to form a tube when it comes to its rapid-decline stage. Cao et al. [8] designed the EMF system can be applied to the attractive forming of a 1-mm-thick AA1060 sheet based on simulation and experiment. Xiong et al. [8] proposed a novel method that uses electromagnetic attraction for tube bulging, and the influence of the discharge parameters has been discussed to improve the forming efficiency. Although the method could ease the difficulty to form a small-size tube, there was still a bottleneck in this method. The tube would collide to the inside layer of the coil and lead to an unsatisfactory forming result. To avoid a potential collision, the inner diameter of the coil should be enlarged. And this would contribute to an undesired attenuation of the attractive force, since the distance between the coil and the tube was increased. So there was a dilemma in this method.

Based on the two methods above, this paper presented an improved dual-coil electromagnetic forming system, in which a dual-coil was placed at the end of the tube instead of outside or inside the tube. This system consisted of two power supplies and a dual coil, and the discharge currents were precisely controlled to generate a Lorentz force to form the tube. To verify the effectiveness of this method, firstly, the forming principle of the electromagnetic flanging was analyzed theoretically. Secondly, an electromagnet-structure full coupling model was developed to simulate the deformation of the tube and a convictive result was obtained. Finally, the influence of the pulse widths of discharge currents was discussed.

2 Basic principles of radial electromagnetic force

In the electromagnetic forming process, when the pulse current flowed through into the driving coil, a pulsed magnetic field is generated and an eddy current is induced in the tube. As a result, a huge radial Lorentz force is generated, and its density can be expressed as [1]

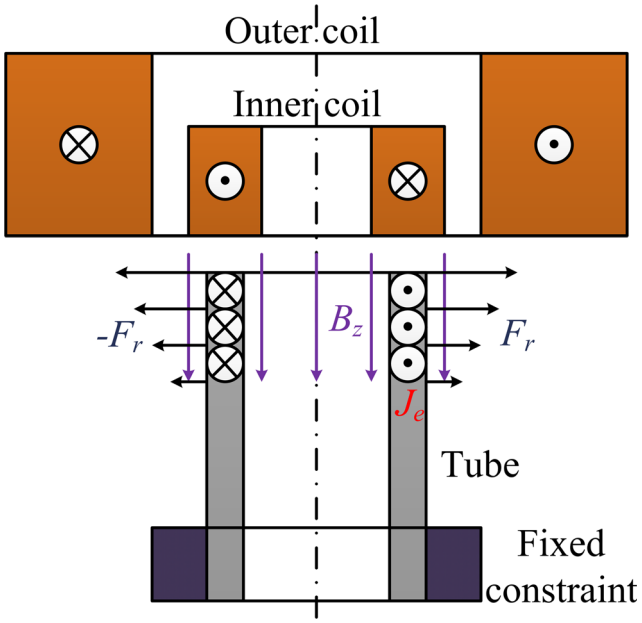

Fig. 2 Schematic of electromagnetic flanging system

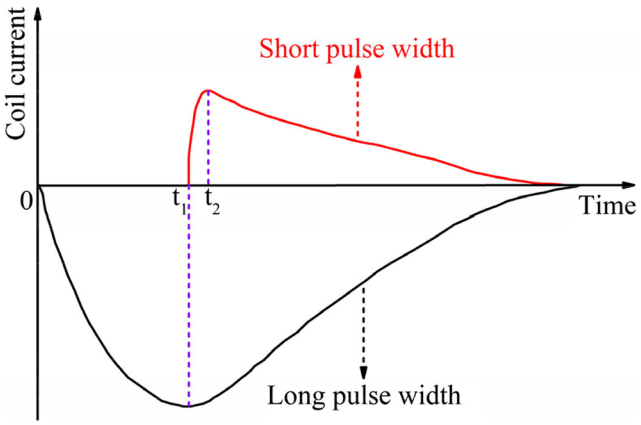

Fig. 3 Schematic diagram of a dual-coil current

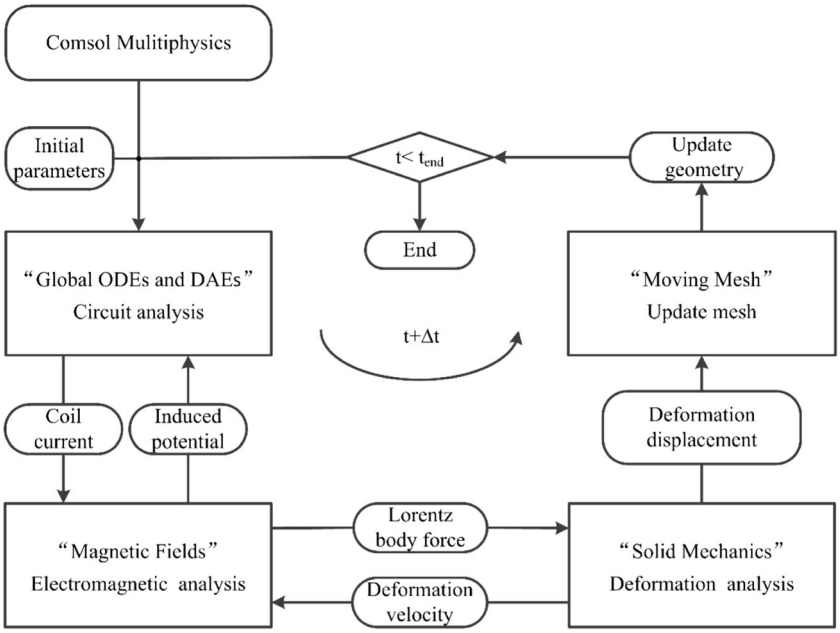

Fig. 4 Flowchart of the implemented algorithm [10]

$$f = J_e \times B \tag{1}$$

where J_e and B are eddy currents density in the circle direction and magnetic flux density respectively.

Lorentz force can be decomposed into the axial and radial component in the analysis of an electromagnetic forming process, which are called as radial Lorentz force and axial Lorentz force, and their densities are determined by [8]

$$f_r = J_e \times B_z \tag{2}$$

$$f_z = -J_e \times B_r \tag{3}$$

where B_r and B_z are the axial component and the radial component of the magnetic flux density respectively.

Electromagnetic flanging requires a radial outward force at the end of the tube. When an eddy current density in the clockwise direction interacts with an axial downward magnetic field, a radial Lorentz force would be generated according to Eq. (2). The schematic drawing of electromagnetic flanging system used in this work is presented in Fig. 2. And the discharge current is shown in Fig. 3, which is a compound of a long pulse width current and a short pulse width current. What's more, the directions of the two currents are opposite, and they are loaded into the outer coil and the inner coil respectively. So radial Lorentz force density in Eq. (2) can be replaced by

$$f_r = \begin{cases} J_{e\text{–long}} \times \left(-B_{z\text{–long}}\right)(t < t_1) \\ -\left(J_{\text{e–short}} - J_{e\text{–long}}\right) \times \left(-B_{z\text{–long}} + B_{z\text{–short}}\right)(t > t_1) \end{cases} \tag{4}$$

where $J_{e\text{-short}}$ and $J_{e\text{-long}}$ are eddy current densities respectively induced by the short pulse current and the long pulse current. $B_{z\text{-long}}$ and $B_{z\text{-short}}$ are axial magnetic fields generated by the long pulse and the short pulse discharge current respectively.

According to Fig. 3, the following inferences can be drawn

$$t_1 \gg t_1 - t_2 \Rightarrow J_{\text{e–short}} \gg J_{e\text{–long}} \tag{5}$$

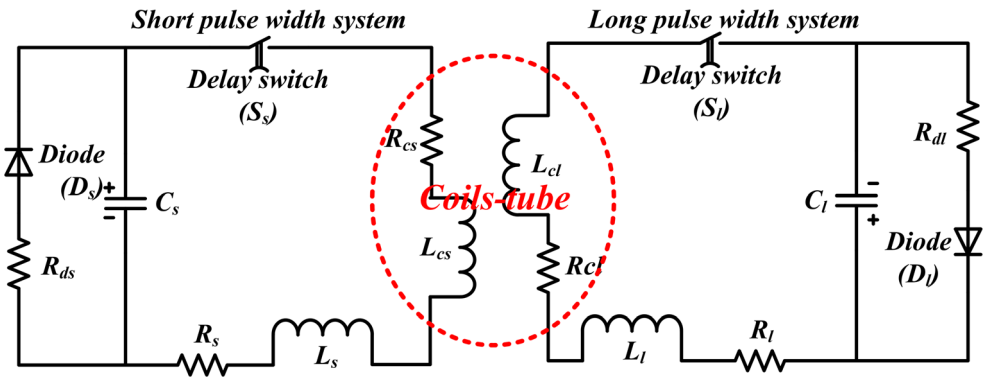

Fig. 5 Schematic diagram of the circuits

Table 1 Circuit parameter

Description	Short pulse width system		Long pulse width system	
	Symbol	Value	Symbol	Value
Initial discharge voltage	U_s	5.8 kV	U_l	6 kV
Capacitance	C_s	80 μF	C_l	3.2 mF
Line inductance	L_s	8.9 μH	L_l	0.33 mH
Line resistance	R_s	8.8 mΩ	R_l	0.1 Ω
Crowbar resistance	R_{ds}	10 mΩ	R_{dl}	0.2 Ω
Coil inductance	L_{cs}	1.1 μF	L_{cl}	70 μH
Coil resistance	R_{cs}	1.2 mΩ	R_{cl}	15 mΩ

$$\left.\begin{array}{l} I_{\text{long-max}} \gg I_{\text{short-max}} \\ N_{\text{long}} \geq N_{\text{short}} \end{array}\right\} \Rightarrow B_{z\text{-long}} \gg B_{z\text{-short}} \tag{6}$$

where t_1 and t_2 are the time when the long pulse and the short pulse current come to their peak, respectively. $I_{\text{long-max}}$ and $I_{\text{short-max}}$ are peak values of the currents. N_{long} and N_{short} are the numbers of turns of the outer coil and the inner coil respectively.

Therefore, f_r can be expressed by

$$f_r \approx -J_{\text{e-short}} \times \left(-B_{z\text{-long}}\right) \tag{7}$$

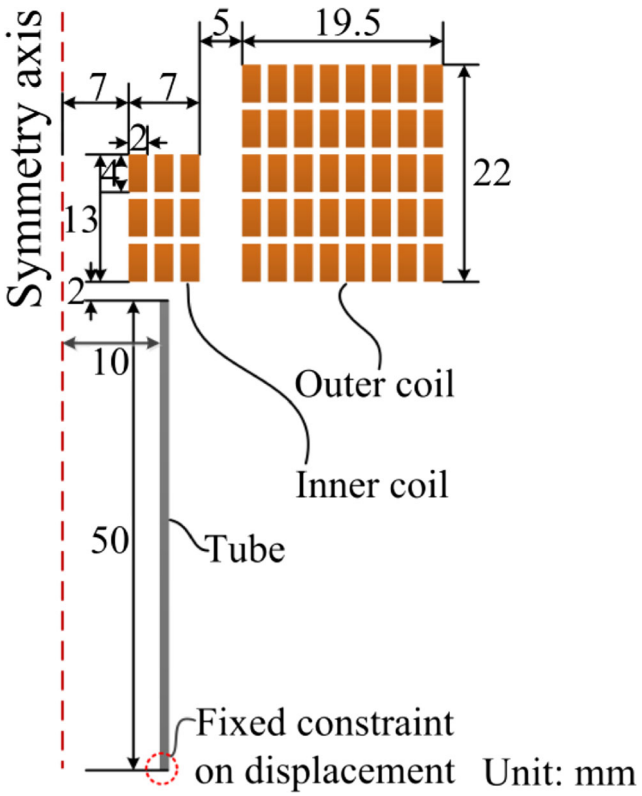

Fig. 6 Geometric model of simulation

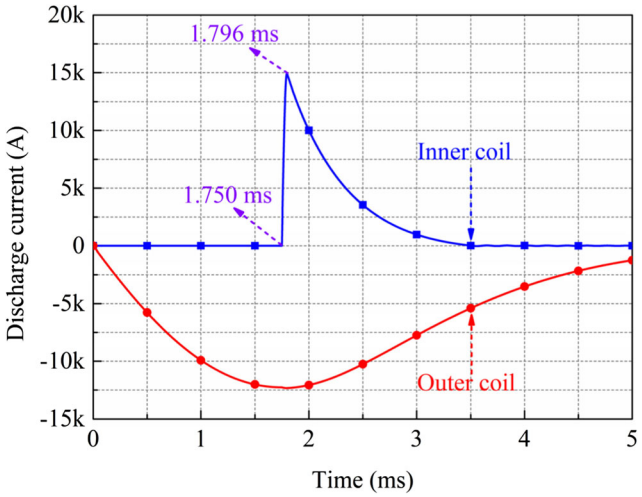

Fig. 7 Waveforms of discharge currents in different branches

That means the outer coil is used to generate a background magnetic field in the axial direction, and inner coil is used to induce eddy current. And the interaction between them can generate the Lorentz force needed for deformation.

3 Simulations

In this section, a numerical simulation model was developed by COMSOL Multiphysics. It was a 2D axisymmetric full-coupled model, taking into account the influence of the sheet displacement and the velocity, the flowchart of the implemented algorithm is illustrated in Fig. 4 [10, 11].

3.1 Circuits

According to the principle described above, the discharge current in this method was similar to [9], and its specific circuit model was shown in Fig. 5. The system consists of two sets of power supply, which drove the inner and the outer coil with precise time-control to generate a required Lorentz force. And their parameters were shown in Table 1.

3.2 Coils

Electromagnetic field model consisted of three parts—the inner coil, the outer coil, and the tube. Its spatial distribution was given in Fig. 6. The distance between inner coil and tube was 2 mm, and the distance between the inner coil and the outer coil was 5 mm. The wire was a 2 mm × 4 mm copper wire, and the layer spacing and the turns' spacing were 0.5 mm. The specific parameters are represented in Fig. 5.

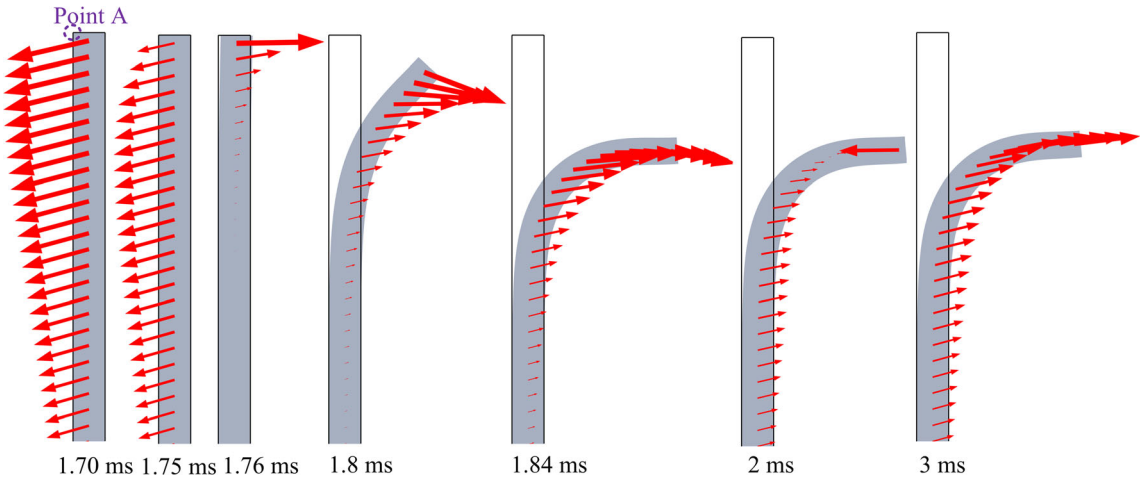

Fig. 8 Distribution of Lorentz force vector at the end of the tube

3.3 Material

In the experiment, an AA1060 tube with a radial of 10 mm and a thickness of 1 mm was adopted. Its elastic modulus was 69 GPa, the Poisson ratio was 0.33 and the initial yield tensile strength was 98 MPa. The stress-strain relationship of this material was derived from [9].

Since the strain rate in electromagnetic forming was very high and it had a great influence on the final forming effect, a Cowper-Symonds constitutive model was adopted to analyze the deformation of the tube. The model was as follows [12].

$$\sigma = \sigma_y \left[1 + \left(\frac{\dot{\varepsilon}}{C}\right)^m\right] \tag{8}$$

where σ_y and $\dot{\varepsilon}$ are yield stress (MPa) and the plastic strain rate (s^{-1}) respectively. For aluminum alloy, $C = 6500\ s^{-1}$, $m = 0.25$.

4 Result and discussion

To verify the effectiveness of this method, a series of simulations were carried out, and the results were presented in the following sections.

4.1 Deformation

Figure 7 shows the discharge currents waveforms of the inner and the outer coils in simulation. It could be seen that they were similar to Fig. 3 in the principal part. The long pulse current reached to its peak at 1.750 ms, and it was the exact time when the short pulse current with a pulse width of 92 μs was loaded in to the inner coil.

Figure 8 shows the distribution of Lorentz force vector in the process of electromagnetic flanging. It could be seen that (1) the Lorentz force reversed when the short pulse width current was discharged into the inner coil (1.76 ms). (2) The

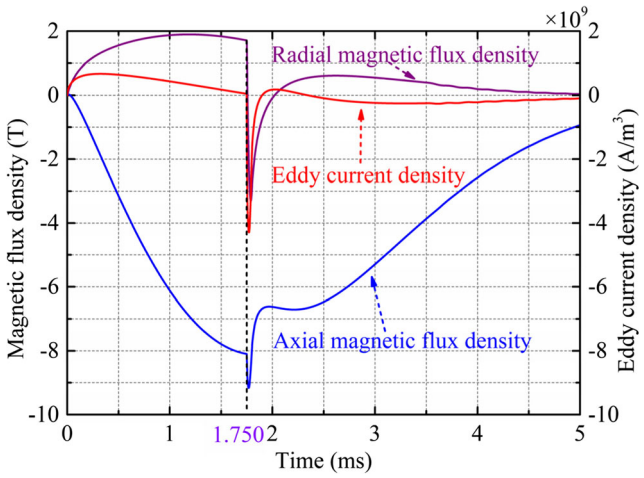

Fig. 9 Calculated magnetic flux density and eddy current density at point A

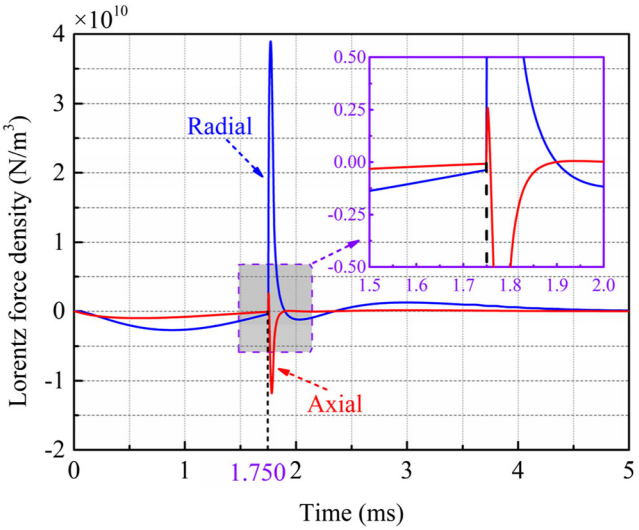

Fig. 10 Calculated magnetic force density at point A

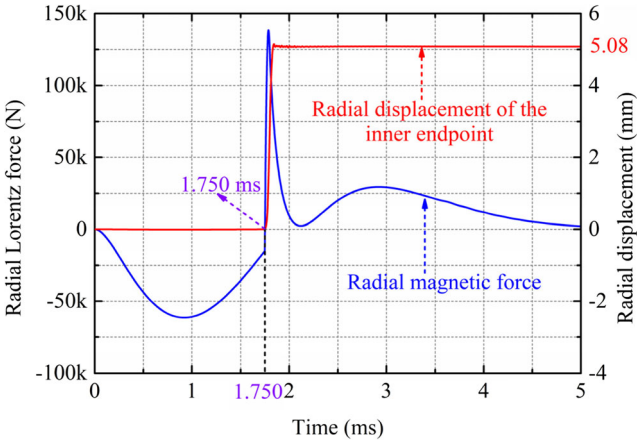

Fig. 11 Calculated radial Lorentz force and radial displacement

Lorentz force at the upper end of the tube was larger than which at the lower end of the tube. Therefore, in this simulation, the Lorentz force we designed matched the forming force required for the electromagnetic flanging.

According to Eq. (7) and the simulation, it could be seen that a required radial Lorentz force should be induced by a circumferential negative (set clockwise as positive) eddy current interacting with an axial downward (negative) magnetic flux density. To prove this assumption, the variation of Lorentz force density at point A in Fig. 8 was analyzed in detail. Figure 9 shows magnetic flux density and eddy current density at point A. It could be seen that the axial background magnetic field generated by the outer coil reaches its maximum at 1.750 ms, which was the exact time when the short pulse width current was discharged into the inner coil and induced a circumferential eddy current. As a result, a huge radial Lorentz force was generated at the upper end of the tube since 1.750 ms, as shown in Fig. 10. In addition, as we can see, the radial component of magnetic flux density reversed when inner coil was discharged. Then, this radial component of magnetic flux density generated an axial component of Lorentz force. This was beneficial for flanging, which would be discussed in detail later on.

Figure 11 shows the calculated results of radial displacement at point A and the radial Lorentz force acted on the tube

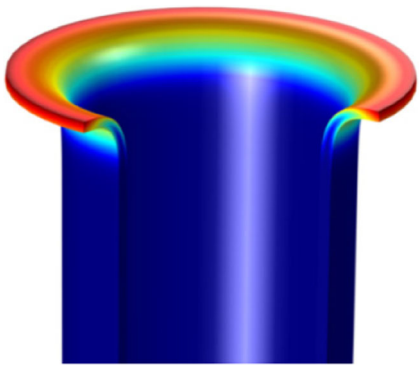

Fig. 12 3D simulation deformation diagram

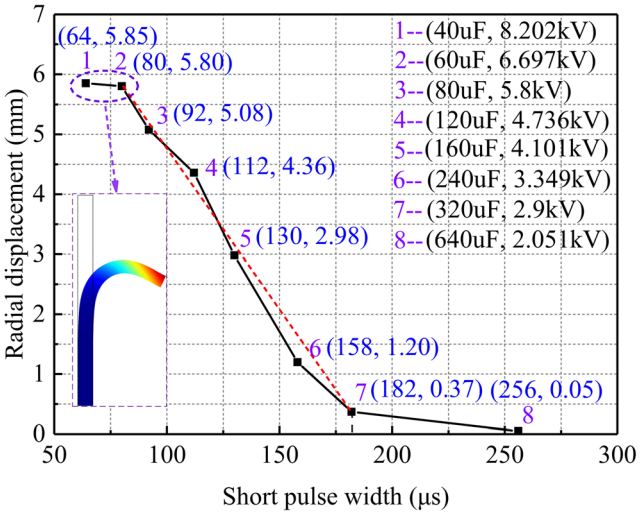

Fig. 13 The relationship between the short pulse width and the radial displacement at point A

in the forming process. It could be witnessed that the radial electromagnetic force acted on the tube was negative when $t <$ 1.750 ms, but it was not sufficient to deform the tube. When $t >$ 1.750 ms, the direction of the radial Lorentz force on the tube reversed to positive and its value increased rapidly, which made the deformation of the tube possible. Furthermore, the final radial displacement was 5.08 mm at point A, and the final deformation of the tube is shown in Fig. 12.

From what we had discussed above, we could draw the conclusion that by placing a dual-coil at the end of the tube could the electromagnetic flanging deformation of small size tube be realized.

4.2 The influence of short pulse width

The analysis above showed that the long pulse width current was mainly to generate background magnetic field and the

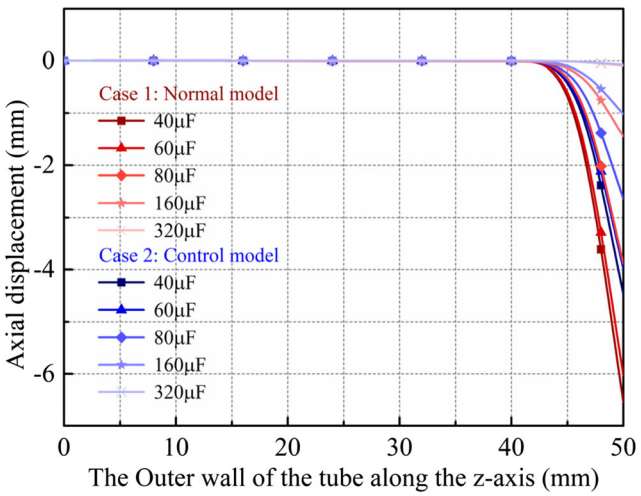

Fig. 14 The axial displacement in the out wall of the tube in different case

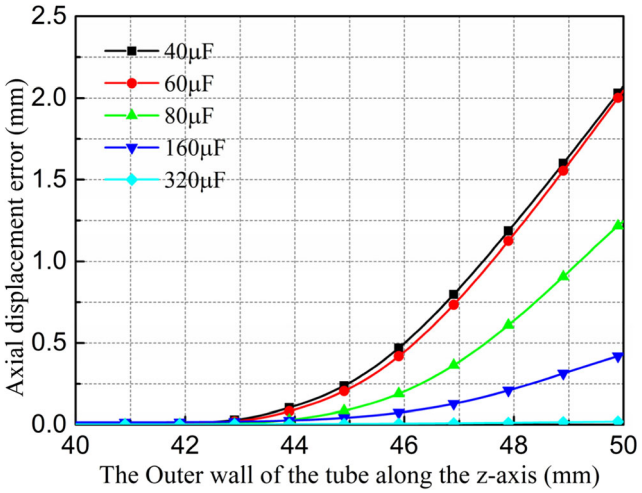

Fig. 15 The axial displacement error between 40−50 mm in different cases

short pulse width was mainly to induce eddy current. As shown in Fig. 7, when $t_1 \gg t_2 - t_1$, the long pulse current had little effect on electromagnetic flanging. But the short pulse current had great influence on the final deformation. Therefore, the influence of the pulse width of the short pulse current was analyzed in detail. A series of simulations under different pulse width of the short pulse current were carried out, while the peak value of the current and the total energy (1.345 kJ) were fixed to certain values.

Figure 13 shows the relationship between the pulse width of the short pulse current (defined as W_s) and the radial displacement. It could be seen that there was a negative correlation between the radial displacement and the pulse width W_s. And the displacement came to nearly 0 when $W_s > 256$ μs, although the background magnetic field remained unchanged. That means it was hard to deform the tube if the short pulse current was not "so short" (in our simulation, it means $W_s >$ 256 μs). The reason was that the eddy current in this situation was too weak to generate enough Lorentz force for forming the tube. However, if the short pulse was "over short" (when $W_s < 80$ μs), the radial displacement was nearly unchanged. The main reason was that the reduction of the width of current would lead to a decline of the duration of the force, then accounted for a saturation in Fig. 12 (when $W_s < 80$ μs).

Besides the radial displacement, there would be an axial displacement in electromagnetic flanging because there was an axial Lorentz force. To discuss it, two types of simulations were carried out. One was the "normal model" just like the model used above, the other was the "control model," in which the axial Lorentz force was manually set to 0. The results are shown in Figs. 14 and 15. It could be seen clearly that the axial displacement was larger than which in "control model." That means the axial Lorentz force generated in this method was helpful for electromagnetic flanging. The main reason was that a huge axial Lorentz force was generated by the cooperation of the radial magnetic field and the eddy current when the magnetic field reached a peak in forming process.

However, the axial Lorentz force could be harmful in some cases. There would be an undesired over-deformation when $W_s < 92$ μs, as shown in Fig. 13. The main reason was that the axial Lorentz force continued to drive the axial deformation of the tube even when the radial deformation was close to saturated. And as we could infer from Eq. (3), there was a negative relationship between the amplitude of this axial Lorentz force and the pulse width of the short pulse current. So there was a dilemma whether the pulse width should be designed to a small value. And in our simulations, the best pulse width for the tube to achieve as large as possible radial displacement without undesired over-deformation was 92 μs.

5 Conclusions

To achieve the electromagnetic flanging of the small-size tube, a dual-coil electromagnetic forming method was presented. Both theoretical analysis and simulation results showed that an appropriate Lorentz force could be obtained by positioning the two coils at the end of the tube and discharging them with special and precise match in timing, thus contributing to an effective deformation. What's more, the negative correlation between the pulse width of discharge current and the radial displacement at the end of the tube was found and discussed through a set of comparative simulations. Besides, the saturation in this negative correlation was discovered and regarded as a result of distinguishing effects of Lorentz force and action time. All these results could significantly facilitate the verification of electromagnetic flanging of small-size tubes. And be conductive to the expansion of electromagnetic forming technology.

Acknowledgments I would like to thank Chistear Ahmed Khan for his contribution in the writing process.

Funding information This work was sponsored by Research Foundation of Education Bureau of Hubei Province, China (Z2017030, Q20171210) and Research Fund for Excellent Dissertation of China Three Gorges University (2018SSPY071).

References

1. Psyk V, Risch D, Kinsey BL, Tekkaya AE, Kleiner M (2011) Electromagnetic forming—a review. J Mater Process Technol 211(5):787–829. https://doi.org/10.1016/j.jmatprotec.2010.12.012
2. Qiu L, Xiao Y, Deng CZ, Li ZX, Xu YH, Li ZH, Chang P (2017) Electromagnetic-structural analysis and improved loose coupling

method in electromagnetic forming process. Int J Adv Manuf Technol 89(1–4):701–710. https://doi.org/10.1007/s00170-016-9071-9

3. Yu HP, Jiang HW, Li CF (2012) Investigations on flanging of aluminum alloy tube under pulsed magnetic force. J Iron Steel Res Int 19:438–441 http://www.cnki.net/kcms/doi/10.13228/j.boyuan.issn1006-706x.2012.s1.088.html
4. Cui XH, Mo JH, Li JJ, Xiao XT (2017) Tube bulging process using multidirectional magnetic pressure. Int J Adv Manuf Technol 90(5–8):2075–2082. https://doi.org/10.1007/s00170-016-9498-z
5. Cao QL, Li ZH, Lai ZP, Li ZZ, Han XT, Li L (2018) Analysis of the effect of an electrically conductive die on electromagnetic sheet metal forming process using the finite element-circuit coupled method. Int J Adv Manuf Technol 1–15. https://doi.org/10.1007/s00170-018-2798-8
6. Li Z, Liu SJ, Li JP, Wang M (2018) Effect of coil length and relative position on electromagnetic tube bulging. Int J Adv Manuf Technol 97:379–387. https://doi.org/10.1007/s00170-018-1779-2
7. Li JJ, Qiu W, Huang L, Su HL, Tao H, Li PY (2018) Gradient electromagnetic forming (GEMF): a new forming approach for variable-diameter tubes by use of sectional coil. Int J Mach Tool Manu 135:65–77. https://doi.org/10.1016/j.ijmachtools.2018.08.005
8. Cao QL, Lai ZP, Xiong Q, Chen Q, Ding TH, Han XT, Li L (2017) Electromagnetic attractive forming of sheet metals by means of a dual-frequency discharge current: design and implementation. Int J Adv Manuf Technol 90(1–4):309–316. https://doi.org/10.1007/s00170-016-9329-2
9. Xiong Q, Tang HT, Deng CZ, Li L, Qiu L (2018) Electromagnetic attraction-based bulge forming in small tubes: fundamentals and simulations. IEEE Trans Appl Supercond 28(3):1–5. https://doi.org/10.1109/TASC.2017.2785778
10. Cao QL, Li L, Lai ZP, Zhou ZY, Xiong Q, Zhang X, Han XT (2014) Dynamic analysis of electromagnetic sheet metal forming process using finite element method. Int J Adv Manuf Technol 74(1–4):361–368. https://doi.org/10.1007/s00170-014-5939-8
11. Qiu L, Yu YJ, Xiong Q, Deng CZ, Cao QL, Han XT, Li L (2018) Analysis of electromagnetic force and deformation behavior in electromagnetic tube expansion with concave coil based on finite element method. IEEE Trans Appl Supercond 28(3):1–5. https://doi.org/10.1109/TASC.2017.2789287
12. Mamalis AG, Manolakos DE, Kladas AG, Koumoutsos AK (2006) Electromagnetic forming tools and processing conditions: numerical simulation. Mater Mauf Process 21(4):411–423. https://doi.org/10.1080/10426910500411785